Supporting Information

Layered-perovskite oxides with *in-situ* exsolved Co-Fe alloy nanoparticles as highly efficient electrode for high-temperature carbon dioxide electrolysis

Xiang Sun[a], Yongjian Ye [a], Mengzhen Zhou[a], Huijun Chen[a], Ying Li[a], Peirong Chen[a], Dehua Dong[b], Yihan Ling[c], Majid Khan[d], Yan Chen*[a]

Material Synthesis：

The solid-state reaction method was used to synthesis the double perovskite $Sr_2Ti_{0.8}Co_{0.2}FeO_{6-\delta}$ (STCF) as described elsewhere.[1,2] The stoichiometric of STCF sample was prepared by mixed the stoichiometric ratio powders of $SrCO_3$, TiO_2, Co_3O_4, Fe_2O_3 (Macklin, China) and appropriate amount of ethanol as solvent together in ball mill to grind for 24 h. Then, placing the dried powder sample in a high temperature muffle furnace and the mixture were calcined at 1200 °C for 8 h in air with a heating rate of 2 °C min^{-1}.

The same preparation method for STCF fuel electrode was used to synthesize the $La_{0.7}Sr_{0.3}CoO_{3-\delta}$ (LSC) oxygen electrode. The precursor, which was mixed the stoichiometric ratio powders of La_2O_3, sintering in air at 1000 °C for 2 hours to remove absorbed water, $SrCO_3$, CO_3O_4 (Macklin, China) and ethanol, was put into ball mill for 8 h. The dried mixture was then sintered at 1000 °C for 6 h in air to form perovskite LSC powders.

The electrochemical performance was acquired using an electrolyte-supported single cell. The electrolyte material is $La_{0.8}Sr_{0.2}Ga_{0.83}Mg_{0.17}O_{3-\delta}$ (LSGM) since its higher ionic conductivity and well stability. The LSGM powders were prepared by the solid-state reaction as described in literature.[3] Before the synthesis, La_2O_3 and MgO were sintered in air at 1000 °C for 2 hours to remove absorbed water. The obtained La_2O_3 and MgO were mixed with $SrCO_3$ and Ga_2O_3 powders (Macklin, China) for further reaction. Powders were dissolved in ethanol and ball-milled for 24 hours, and LSGM electrolyte precursor was prepared after drying, then the precursor was sintering at 1450 °C for 10 hours to achieve perovskite phase powders (LSGM powders).

CO_2-TPD test methods

Temperature-programmed desorption of CO_2 (CO_2-TPD) was tested on tubular furnace with an on-line quadrupole mass spectrometer (HAS-301-1340, Hiden Analytical Ltd.). First, 200 mg samples were pretreated in a quartz tube at 600 °C for 1 h in N_2 atmosphere with a flow rate of 30 mL min^{-1}. The heating rate was 10 °C min^{-1}. For the CO_2-TPD measurement, the pretreated samples were firstly exposed to 100% CO_2 for 1 h with a gas flow rate of 30 mL min^{-1} at room-temperature. The tube was then swept with pure N_2 (30 mL min^{-1}) for 1 h to remove any residual CO_2 gas. Thereafter, the sample was heated from 50 to 800 °C in pure N_2 and the desorption of CO_2 as a function of heating temperature was detected using the mass spectroscopy.

Electrolysis Cell Fabrication

The CO_2 electrolysis performance were evaluated using an electrolyte-supported single cell. To obtain a denser electrolyte pellet, we carried out a two-step sintering process. The LSGM electrolyte precursor was pressed into an condense pellet and pre-sintered at 1250 °C for 10 h. The obtained pellet was ground into powders and were then pressed into pellet again. After further sintering at 1450 °C for 10 h, the LSGM electrolyte was successfully prepared. The fuel electrode slurry was prepared by mixing STCF, SDC and graphite in a weight ratio of 5:5:1: with a binder composed of α-terpineol and Polyvinyl Butyral, followed by ground with mortar for 3 h. The mass ratio of powders to colloid was 1.2:1. The oxygen electrode slurry composed of LSC and SDC was prepared using similar approach as the fuel electrode. The PrOx impregnation solution was prepared by dissolved $Pr(NO_3)_3 \bullet 6H_2O$ in appropriate amount of mixture solution consist of ethanol, ethylene glycol, 2-butoxy ethanol and H_2O, and the concentration of impregnates is 1mol L^{-1}.

The fuel electrode ink (STCF-SDC) was brushed on the one side of prepared electrolyte pellets, and co-fired at 1150 °C for 3 h. Then, the oxygen electrode slurry (LSC-SDC) was coated on the other side of LSGM, followed by sintering at 1100 °C for 2 h. Moreover, the PrOx impregnation solution was impregnated on the oxygen electrode side several times, with a total volume of 10 μL. Finally, the complete electrolyte-supported single cell was achieved after calcined at 500 °C for 1 h, denoted as STCF-SDC/LSGM/LSC-SDC-PrOx. Ag grid was painted onto the surfaces of both sides of electrode surface as current collector layer. The electrode effective area of every cell was 0.2 cm^{-}

[2].

Faraday efficiency calculation

$$FE_{CO} = \frac{nFVvp_0}{RT_0 I} \times 100\%$$

Where the,

R and *F* are Molar gas constant and faraday constant, respectively.

n is the number of electrons transferred in the reaction.

v (Vol%) = volume concentration of CO in the exhaust gas from the cell (GC data).

V (mL/min) = gas flow rate value of gas flowmeter connected to the reaction chamber of electrolytic cell at room temperature and under ambient pressure.

I (A) = steady-state cell current.

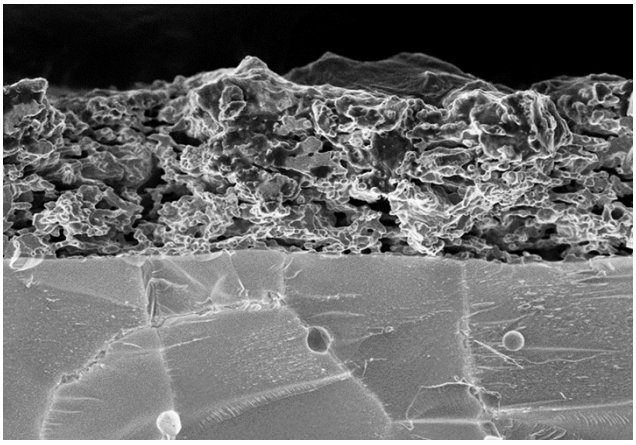

Fig. S1 SEM image of pure STCF electrode material without SDC.

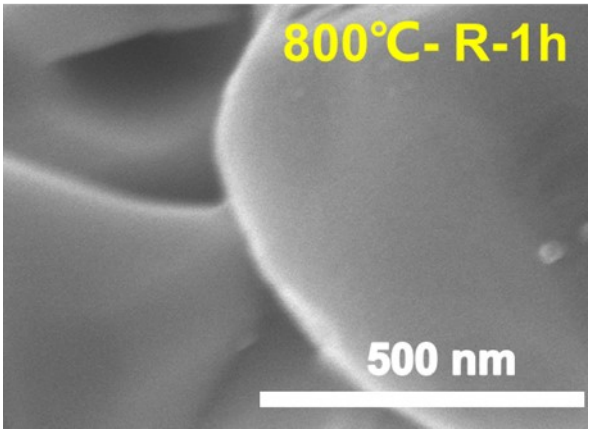

Fig. S2 SEM patterns of STCF after reduction treatment at 800 °C for 1 h.

From the point scan, five elements (Sr, Ti, Co, Fe and O) were observed in the Co-Fe-STCF material, and no other impurity elements presented (Fig. S3).

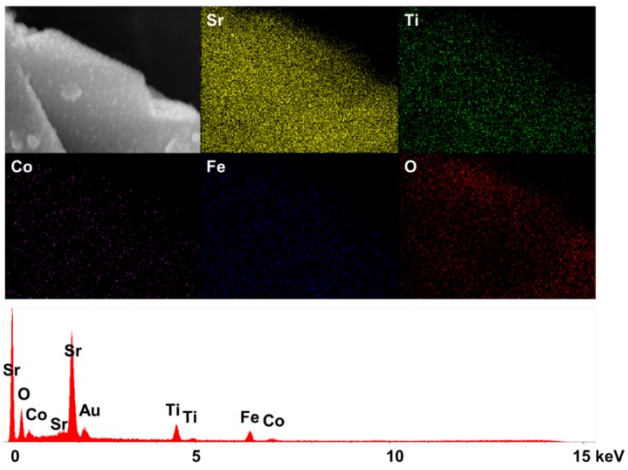

Fig. S3 SEM image and elemental maps and point scan of Co-Fe-STCF.

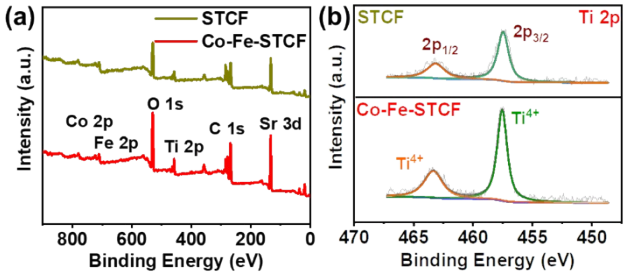

Fig. S4 XPS spectra of survey **(a)**, and Ti 2p **(b)** for STCF and Co-Fe-STCF.

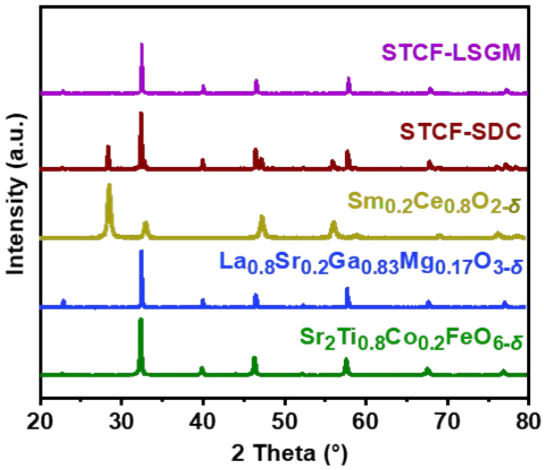

Fig. S5 A chemical compatibility results of STCF with LSGM and SDC, respectively, after calculating at 1150 °C for 10 h in air.

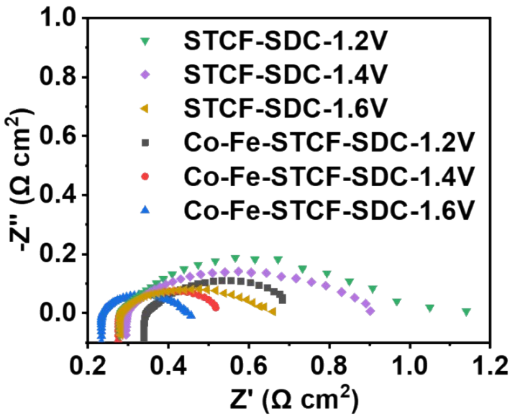

Fig. S6 EIS curves of SOEC with different fuel electrode at different potentiostatic voltages at 800 °C.

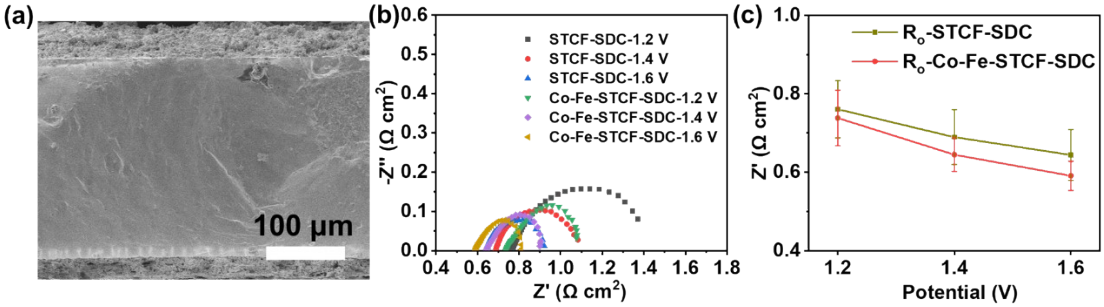

Fig. S7 (a) SEM of the cross section of another cell with STCF-SDC electrode **(b)** EIS curves of another sets of cells with STCF-SDC and Co-Fe-STCF-SDC electrode at different potentiostatic voltages at 800 °C and **(c)** The average ohmic resistance (Ro) of different cells under the same voltage with the error bar representing the deviation of difference cells. The Ro value decreased as the applied potential got more negative. Such phenomena are likely due to the reduction of electrode material under negative potential. The reason why the Co-Fe-STFC change more apparently with applied potential is still not clear and require further investigation.

After 100 h high temperature electrolysis stability test in carbon dioxide, the microstructure of electrolyte/electrode interface has changed and is no longer dense (Fig. S8).

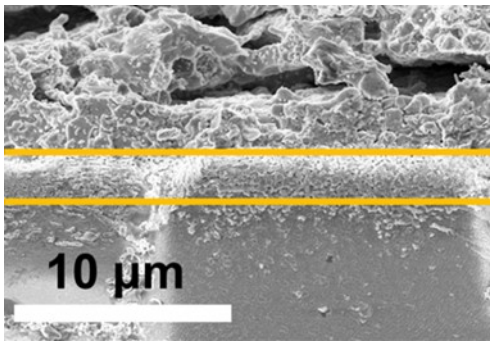

Fig. S8 SEM patterns of cell cross section after the stability test 800 °C for 100 h.

Table S1. XPS analysis of $2p_{3/2}$ for Co and Fe elements.

Elements	B.E. $2p_{3/2}$ (eV)			0 (at.%)	2+ (at.%)	3+ (at.%)
	0	2+	3+			
Co	777.8	780.15	781.8	8.33	50.00	41.67
Fe	706.6	710.1	711.9	4.56	41.50	53.94

Table S2. The performance of representative materials for electrolysis of pure carbon dioxide.[4-22]

Exsolved Metal	Oxide Matrix Composition	T (°C)	Gas Composition	Potential (V)	Current Density (A cm^{-2})	CO Production Rate (ml min^{-1} cm^{-2})	Ref.
-	$SrFeO_{3-\delta}$-Ni	800	CO_2	1.6	0.75	4.8	[4]
-	$La_{0.75}Sr_{0.25}Cr_{0.5}Mn_{0.5}O_{3-\delta}$	800	CO_2	1.5	0.09	1	[5]
-	$La_{0.75}Sr_{0.25}Cr_{0.5}Mn_{0.5}O_{3-\delta}$-$V_2O_5$	800	CO_2	1.5	0.21	1	[6]
-	$La_{0.75}Sr_{0.25}Cr_{0.5}Mn_{0.5}O_{3-\delta}$-NiCu	800	CO_2	1.6	0.782	5.32	[7]
-	$La_{0.6}Sr_{0.4}Fe_{0.9}Mn_{0.1}O_{3-\delta}$	800	CO_2	1.6	0.68	4.319	[8]
-	$La_{0.6}Sr_{0.4}Fe_{0.8}Ni_{0.2}O_{3-\delta}$	800	CO_2	1.6	0.629	4.08	[9]
-	$La_{0.5}Sr_{0.5}Fe_{0.95}V_{0.05}O_{3-\delta}$	800	CO_2	1.6	0.62	4.48	[10]
Ni	$(La_{0.2}Sr_{0.8})_{0.95}Ti_{0.85}Mn_{0.1}Ni_{0.05}O_{3-\delta}$	800	CO_2	2.0	0.87	3.7@1.6V	[11]
Ni	$(La_{0.75}Sr_{0.25})_{0.9}(Cr_{0.5}Mn_{0.5})_{0.9}Ni_{0.1}O_{3-\delta}$	800	CO_2	2.0	0.38	1.0@1.5V	[12]
Ni	$Sr_2Fe_{1.45}Ni_{0.05}Mo_{0.5}O_{6-\delta}$	800	CO_2	1.5	0.73	3@1.4V	[13]
Ni	$(La_{0.3}Sr_{0.7})_{0.9}Ti_{0.95}Ni_{0.05}O_{3-\delta}$	800	CO_2	2.0	0.3181	1.3@1.6V	[14]
Fe	$(Sr_{0.95})_{0.9}(Ti_{0.8}Nb_{0.1}Mn_{0.1})_{0.9}Fe_{0.1}O_{3-\delta}$	800	CO_2	2.0	0.3142	1.2@1.6V	[15]
Cu	$(La_{0.75}Sr_{0.25})_{0.9}(Cr_{0.5}Mn_{0.5})_{0.9}Cu_{0.1}O_{3-\delta}$	800	CO_2	2.0	0.477	1.55@1.6V	[16]
Co-Fe	$Sr_2Fe_{1.35}Mo_{0.45}Co_{0.2}O_{6-\delta}$	800	CO_2	1.6	1.2	8.5	[17]
Fe-Ni	$Sr_{1.9}Fe_{1.5}Mo_{0.4}Ni_{0.1}O_{6-\delta}$	800	CO_2	1.5	2.16	1.867@1.3V	[18]
$FeNi_3$	$La_{0.6}Sr_{0.4}Fe_{0.8}Ni_{0.2}O_{3-\delta}$	850	CO_2	2.0	1.42	6@1.6V	[19]
Fe-Ni	$Sr_2Fe_{1.35}Mo_{0.45}Ni_{0.2}O_{6-\delta}$	800	95% CO_2/N_2	1.6	0.934	7.8	[20]
Co-Fe	$La_{0.4}Sr_{0.6}Co_{0.2}Fe_{0.7}Mo_{0.1}O_{3-\delta}$	800	CO_2	1.6	1.45	10.5	[21]
Ni-Cu	$NbTi_{0.5}(Ni_{0.75}Cu_{0.25})_{0.5}O_4$	800	CO_2	1.6	0.113	0.1629@1.4V	[22]
Co-Fe	**$Sr_2Ti_{0.8}Co_{0.2}FeO_{6-\delta}$**	**800**	**CO_2**	**1.6**	**1.26**	**8.75**	**This work**

References

1 B. B. Niu, C. L. Lu, W. D. Yi, S. J. Luo, X. N. Li, X. W. Zhong, X. Z. Zhao and B. M. Xu, *Appl. Catal. B: Environ.*, 2020, **270**, 118842.

2 T. L. Zhu, H. E. Troiani, L. V. Mogni, M. F. Han and S. A. Barnett, *Joule*, 2018, **2**, 478-496.

3 M. Ni, M. K. H. Leung and D. Y. C. Leung, *Int. J. Hydrogen Energy*, 2008, **33**, 2337-2354.

4 C. L. Zhu, S. S. Hou, L. X. Hou and K. Xie, *Int. J. Hydrogen Energy*, 2018, **43**, 17040-17047.

5 S. S. Xu, S. S. Li, W. T. Yao, D. H. Dong and K. Xie, *J. Power Sources*, 2013, **230**, 115-121.

6 X. Z. Zhang, L. T. Ye, J. P. Hu, J. Li, W. H. Jiang, C. J. Tseng and K. Xie, *Electrochim. Acta*, 2016, **212**, 32-40.

7 C. L. Zhu, L. X. Hou, S. S. Li, L. Z. Gan and K. Xie, *J. Power Sources*, 2017, **363**, 177-184.

8 X. Z. Peng, Y. F. Tian, Y. Liu, W. J. Wang, L. C. Jia, J. Pu, B. Chi and J. Li, *J. CO_2 Util.*, 2020, **36**, 18-24.

9 Y. F. Tian, H. Y. Zheng, L. L. Zhang, B. Chi, J. Pu and J. Li, *J. Electrochem. Soc.*, 2018, **165**, F17-F23.

10 Y. J. Zhou, Z. W. Zhou, Y. F. Song, X. M. Zhang, F. Guan, H. F. Lv, Q. X. Liu, S. Miao, G. X. Wang and X. H. Bao, *Nano Energy*, 2018, **50**, 43-51.

11 L. T. Ye, M. Y. Zhang, P. Huang, G. C. Guo, M. C. Hong, C. S. Li, J. T. S. Irvine and K. Xie, *Nat. Commun.*, 2017, **8**, 14785.

12 C. Ruan and K. Xie, *Catal. Sci. Technol.*, 2015, **5**, 1929-1940.

13 S. Q. Hu, L. X. Zhang, H. Y. Liu, W. P. Li, Z. W. Cao, L. L. Cai, Y. Zhu, X. F. Zhu and W. S. Yang, *J. Energy Chem.*, 2019, **36**, 87-94.

14 L. Z. Gan, L. T. Ye, S. W. Tao and K. Xie, *Phys. Chem. Chem. Phys.*, 2016, **18**, 3137-3143.

15 J. Zhang, K. Xie, Y. Zhang, L. M. Yang, G. J. Wu, Q. Q. Qin, Y. X. Li and Y. C. Wu, *RSC Adv.*, 2014, **4**, 22697-22709.

16 H. X. Li, G. H. Sun, K. Xie, W. T. Qi, Q. Q. Qin, H. S. Wei, S. G. Chen, Y. Wang, Y. Zhang and Y. C. Wu, *Int. J. Hydrogen Energy*, 2014, **39**, 20888-20897.

17 H. F. Lv, L. Lin, X. M. Zhang, Y. F. Song, H. Matsumoto, C. B. Zeng, N. Ta, W. Liu, D. F. Gao, G. X. Wang and X. H. Bao, *Adv. Mater.*, 2020, **32**, 1906193.

18 Y. H. Li, B. B. Hu, C. R. Xia, W. Q. Xu, J. P. Lemmon and F. L. Chen, *J. Mater. Chem. A*, 2017, **5**, 20833-20842.

19 Y. F. Tian, L. L. Zhang, L. C. Jia, X. Wang, J. Yang, B. Chi, J. Pu and J. Li, *J. CO_2 Util.*, 2019, **31**, 43-50.

20 H. F. Lv, L. Lin, X. M. Zhang, D. F. Gao, Y. F. Song, Y. J. Zhou, Q. X. Liu, G. X. Wang and X. H. Bao, *J. Mater. Chem. A*, 2019, **7**, 11967-11975.

21 H. F. Lv, T. F. Liu, X. M. Zhang, Y. F. Song, H. Matsumoto, N. Ta, C. B. Zeng, G. X. Wang and X. H. Bao, *Angew. Chem. Int. Edit.*, 2020, **59**, 15968-15973.

22 H. S. Wei, K. Xie, J. Zhang, Y. Zhang, Y. Wang, Y. Q. Qin, J. W. Cui, J. Yan and Y. C. Wu, *Sci. Rep.*, 2014, **4**, 5156.